TECHNICAL MEMORANDUM

242

The ECMWF implementation of three dimensional variational assimilation Part II: Structure functions

F. Rabier, A. McNally, E. Andersson,
P. Courtier, P. Undén, J. Eyre,
A. Hollingsworth and F. Bouttier

Research Department

January 1998

European Centre for Medium-Range Weather Forecasts
Europäisches Zentrum für mittelfristige Wettervorhersage
Centre européen pour les prévisions météorologiques à moyen

The ECMWF implementation of three dimensional variational assimilation (3D-Var) Part II: Structure functions

F Rabier, A Mc Nally, E Andersson, P Courtier, P Undén, J Eyre, A Hollingsworth, F Bouttier

Abstract

The 3D-Var structure functions are evaluated from the statistics of the differences between two forecasts valid at the same time. Results compare satisfactorily with the existing literature. Non-separability of the correlation functions is a pervasive feature. Accounting for non-separability in 3D-Var is necessary to reproduce geostrophic characteristics of the statistics such as the increase of length-scale with height for the horizontal correlation of the mass variable, sharper vertical correlations for wind than for mass and shorter horizontal length-scale for temperature than for mass. In our non-separable 3D-Var the vertical correlations vary with total wavenumber and the horizontal correlation functions vary with vertical level.

1. INTRODUCTION

The companion paper by *Courtier et al* (1998) (Part I) presents the three-dimensional variational analysis scheme as a statistical interpolation algorithm relying on the specification of observation and background (short-range forecast) error covariance matrices. As explained in *Daley* (1991), the correct specification of the background error covariance matrix is important for such a system. The form of this matrix governs the filtering of the observations and the spatial multivariate interpolation of the filtered observations (*Hollingsworth*, 1989), examples of which are presented in the companion paper by *Andersson et al* (1998) (Part III). This part of the paper addresses the problem of specifying those background error characteristics.

Kalman filter includes an equation for the temporal evolution of forecast error statistics. However, due to its heavy computational cost, it cannot presently be applied operationally to large dimension models. Most systems use ad-hoc background error covariance matrix specifications. For example, at ECMWF in the previous Optimum Interpolation system, the background correlations (which are assumed locally homogeneous and isotropic) are kept constant in time and the analysis error variance estimate depends on data coverage. Our specified correlation structures are based on the parallel studies of *Phillips* (1986) and *Hollingsworth and Lönnberg* (1986), *Lönnberg and Hollingsworth* (1986), the latter two papers being referred to as HL86 and LH86 in the rest of the text. *Phillips* (1986) presented a theoretical description of background errors as an ensemble of random slow modes with equipartition of energy. The striking features of the covariance statistics of his system are that the horizontal length-scale for temperature is smaller than that for height, the horizontal length-scale for height increases with altitude, and the vertical correlations are sharper for wind than for mass. Such results agree with the findings of HL86 and LH86, who based their studies on the verification of forecasts against radiosonde data over North America. Some other important results of HL86 and LH86 are that the wind background errors are comparable in magnitude with observation errors and that the background errors are dominated by

the synoptic scales which are largely non-divergent in the troposphere. Background errors for height are also comparable in magnitude with observation errors, and they have a substantial large-scale component for which the vertical structure has a very broad scale. A more recent application of HL86's method by B*artello and Mitchell* (1992) has focused on the non-separability of the statistics. Their three-dimensional model of forecast error covariances, based on Bessel functions in the horizontal and normal modes in the vertical, is successful in reproducing the significant observed increase of horizontal length scale with height. These studies agree in many respects and in particular in the finding that the separable mathematical models misrepresent some important features of the correlations. Until recently a separable framework has been widely used in operational practice for reasons of cost.

Observational studies have been extremely useful to investigate background error statistics and specify some approximations in the Optimum Interpolation system. However, with a global analysis such as the 3D-Var or the SSI used at NCEP (*Parrish and Derber*, 1992), multi-variate covariance information is needed at all wavenumbers of the spectral expansion of the analysis fields. Studies such as HL86 and LH86 used high quality homogeneous radiosonde networks distributed over a continental area such as North America. Since the horizontal extent of North America is about 4000 km, the observational methods cannot provide information for equivalent spherical total wavenumber smaller than approximately 10. Furthermore, although the density of the radiosonde network would allow the specification of the smallest scales used in the analysis for the time being (T63), this will not be true anymore when going to finer resolution in the near future. As far as vertical resolution is concerned, one needs to go from the relatively coarse radiosonde data distribution in the vertical to the model 31 levels, either by interpolation or by modelling of the correlations. These limitations are the main incentives for the development of new methods such as the method used at NCEP which we will call the "NMC method" for historical reasons. The basic strategy of this method, described by *Parrish and Derber* (1992), is to accumulate statistics of the differences between forecasts at different ranges and valid at the same time. The assumption behind the method is that the differences between these forecasts represent forecast error. The main benefits are that it provides global, multi-variate correlations with full vertical and spectral resolution. A description of the "NMC method" is given in section 2, followed by results obtained at ECMWF in section 3. Section 4 discusses the practical implementation of the resulting statistics in the operational 3D-Var system. The advantages and limitations of the method are discussed in section 5.

2. DESCRIPTION OF THE METHOD

The 'NMC' method assumes that the statistics of the differences between forecasts at different ranges valid at the same time are representative of forecast error statistics. A rigorous justification of this assumption is difficult. Some arguments have been proposed by *Bouttier* (1994). In this paper, we concentrate on a posteriori justification, by comparing the results with the existing literature.

For this study the method is applied to comparisons of 24 and 48 hour forecast fields both valid at 12Z on the same day. This choice is somewhat arbitrary, but using the 24 hour forecast as a validation avoids any problems associated with spin-up which could be present in the forecast differences but not in the real forecast error. It also allows differences to be examined over a 24 hour period, which is not so long that the error structure is significantly different from a 6 hour forecast error, and not so short that the forecasts are too similar because of the lack of data to update the starting analysis. Other time-ranges and analysis-lags have been tried (0-24, 0-12, 0-6, 24-36,..). All results are quite comparable, except for the comparison on the shortest time lag 0-6 between the background and the analysis which mainly represents the structure functions used in the OI analysis.

Results will be presented for the basic model variables: T (temperature), $\ln ps$ (logarithm of the surface pressure), wind (rotational and divergent parts), Q (specific humidity). Furthermore, use will be made of the statistics for the mass variable P related to temperature and logarithm of surface pressure through the linearized hydrostatic relation giving P at level l as:

$$P_l = \sum_{i=L}^{l} RT_i \Delta \ln p_i + RT_r \ln p_s \tag{1}$$

where L is the number of vertical levels of the model and T_r is a constant reference temperature (=270 K). A reference pressure equal to 1000 hPa is used in the variation of the logarithm of pressure. Quite a large sensitivity to these reference values was found and the particular values 270 K and 1000 hPa were chosen for their realism when interpreted as mean values. (Using the same values as those used in the integration of the forecast model for the semi-implicit computations, e.g. 300 K and 800 hPa, might be justified for numerical stability reasons, but is not realistic enough to obtain a mass variable P which can be identified with geopotential height.)

For each variable, the operational forecasts were compared for a period of 90 consecutive days extending from December 1992 to February 1993. Statistics for other seasons were computed but results are very stable with season as far as global statistics are concerned. The computations were carried out at the resolution T106L31 where 106 is the number of spherical harmonics in the triangular expansion and 31 is the number of levels (for a reference on the ECMWF model, see for instance Simmons 1991). The mean error field is a full spectral field (locally varying mean) which is removed from each departure field.

As explained in Part I, the covariance matrix is assumed block-diagonal in spectral space.

Expanding a field $x = \sum_{n=0}^{N} \sum_{m=-n}^{n} x_n^m Y_n^m$ in spherical harmonics the total variance for a given wavenumber n is $\sum_{m=-n}^{n} \langle x_n^m x_n^{m*} \rangle = (2n+1)b_n$ where $(x_n^m)^*$ is the conjugate complex of x_n^m and $\langle x \rangle$ is the mathematical expectation.

The quantities $(2n+1)b_n$ provide a variance power spectrum. b_n is the modal variance as introduced in part I, eq (9).

The correlation spectra h_n are deduced from the covariances by normalizing by the global variance:

$$\sigma^2 = \sum_{n=0}^{N} (2n+1)b_n; \quad h_n = \frac{(2n+1)b_n}{\sigma^2} \tag{2}$$

The vertical covariance between two levels is $B^{kl} = \sum_{n=0}^{N} \sum_{m=-n}^{m} \langle (x_{kn}^m)(x_{ln}^m)^* \rangle$. The total vertical correlation between two levels l and k is

$$V^{kl} = \frac{B^{kl}}{\sigma_k \sigma_l} \tag{3}$$

The total covariance $B^k = \sum_{n=0}^{N} B_n^{kl}$ where $B_n^{kl} = \sum_{m=-n}^{n} \langle (x_{kn}^m)(x_{ln}^m)^* \rangle$ is the vertical covariance for wavenumber

$$n, B^{kl} = \sum_{n=0}^{N} \sqrt{B_n^{kk}} \sqrt{B_n^{ll}} \times \frac{B_n^{kl}}{\sqrt{B_n^{kk}} \sqrt{B_n^{ll}}}$$

The vertical correlation at wavenumber n is

$$V_n^{kl} = \frac{B_n^{kl}}{\sqrt{B_n^{kk}}\sqrt{B_n^{ll}}} \tag{4}$$

3. RESULTS

Results obtained from these statistics are presented in the following, with the standard-deviation results in sub-section 3.a, the horizontal correlation results in sub-section 3.b and the vertical correlation results in sub-section 3.c.

3a Variation of standard-deviations

A global factor to re-scale the 24 hr minus 48 hr forecast divergence down to a 6hr forecast error has been found by comparison with statistics of 6hr forecast minus TOVS radiance data (for a reference on the use of TOVS radiance data at ECMWF and the use of statistics related to them, see *Eyre et al* 1993). The resulting value (0.9) is larger than what would be expected, but it should be remembered that a 24hr forecast divergence is not equal to a 24hr forecast error, and that the NMC method relies on a lot of hypotheses which might not be strictly verified. The globally averaged standard-deviations for each horizontal level, after application of this scaling factor, are presented in Fig 1 for variables T, P and U (wind component). The modified P variable shown in the figure will be discussed in section 4. The wind components' standard-deviations are actually obtained by the geostrophic relationship formula $\sigma U = \sigma(P)/fL(P)$, where f is taken as 0.0001 s^{-1}, and $L(P)$ is the length-scale for the mass variable as defined in section 2. Both profiles for U and P agree remarkably well with results from HL86 (Fig 3), LH86 (Fig 2) and *Bartello and Mitchell* (1992) (Figs 3 and 7) with, in particular, a maximum error around the jet level 300 hPa. The pressure levels of the maximum errors are slightly different for height and for wind, which was also the case in *Bartello and Mitchell* (1992). The vertical profile of temperature standard-deviation of error is more markedly different with a maximum slightly higher at 200 hPa.

So far, only the vertical variation of the globally averaged standard-deviations has been mentioned. The horizontal variation of the estimated standard-deviations for temperature at level 18 (500 hPa) is presented in Fig 2. These statistics appear to be quite noisy, although three months of accumulation of statistics went into their calculation. They also have a tendency to go to low values in the tropics, where not so many data are available, and the time variability of the atmosphere is lower which causes "NMC method" to break down. For these reasons, this horizontal variation is not used in practice (see section 4 for an explanation of what is actually used). However, it should be mentioned that this pattern of standard-deviations displayed in Fig 2 shows that the globally averaged statistics obtained with this method are mainly representative of mid-latitudes where standard-deviations have large values, with even more weighting from the Southern Hemisphere than from the Northern Hemisphere. The covariance matrices obtained with the NMC method and discussed below should then agree reasonably well with balanced statistics. In particular, one can expect to find in these statistics some of the features discussed in the ensemble of slow modes described by *Phillips* (1986). In his paper, the statistics obtained with these balanced modes are such that the horizontal length-scale for temperature is smaller than that for height, the horizontal length-scale for height increases with altitude, and the vertical correlations are sharper for wind than for mass. In the following section we shall see that this is indeed the case.

3b Horizontal correlations

Horizontal correlations were examined for each vertical level and for each variable. Figure 3 presents auto-correlation spectra for selected variables and levels, namely level 6 (roughly 100 hPa) shown as dash-dotted lines, 10 (200 hPa) shown as long-dashed lines, level 18 (roughly 500 hPa) shown as solid lines and level 26 (850 hPa) shown as dashed lines.

Figure 3,a shows the auto-correlation spectra for the mass variable P, derived from the covariances for temperature and surface pressure. All spectra peak at around wavenumber 6 to 10, which corresponds to synoptic scales. However, the different behaviour of the "stratospheric" levels 6 and 10 compared to the "tropospheric" ones is quite noticeable. The "stratospheric" levels tend to have more energy in the large scales (wavenumbers less than 10) and much less energy in the small scales (wavenumbers greater than 10). On the other hand, tropospheric levels behave fairly similarly, with a slope around -3.2 in the wavenumber range 20 to 60, and around -4.5 in the wavenumber range 60 to 100. A comparison with previous results using expansion in terms of Bessel functions can be made using the equivalence between the two different types of expansion detailed in Part I. The equivalent slopes in power spectra found by *Lönnberg* (1988) and *Bartello and Mitchell* (1992) are -3 and -3 to -4. One can then conclude that these spectra estimated from the NMC method agree reasonably well with the literature for the wavenumber range 20 to 60. For smaller scales, it is difficult to compare with the results of previous studies, as the direct computation of the statistics of background minus observations did not allow a precise description in the range 60 to 100. This can for instance be noticed in the noise present in Fig 7 of LH86 for scales smaller than n=60.

Following HL86 and *Daley* (1991), one can derive the "kinetic energy spectra" from stream function ψ and velocity potential χ statistics, or equivalently vorticity and divergence statistics, independently:

$$(B_{l,l} + B_{t,t})_{\psi} = -\Delta(B_{\psi\psi}) \tag{5}$$

$$(B_{l,l} + B_{t,t})_{\chi} = -\Delta(B_{\chi\chi})$$

knowing that the sum of the two will give the full kinetic energy statistics (Δ is the Laplacian operator, l indicates the longitudinal component of the wind and t the transverse component of the wind as in HL86 and LH86). The spectra derived from the vorticity and divergence statistics are shown in Fig 3, panels b and c respectively. Compared with the mass spectra, these wind statistics have more weight in the small scales (high wavenumbers). As shown in Table 1, the slopes are smaller in the inertial range. The spectra derived from the divergence statistics (Fig 3,c) are even flatter with slopes of around -0.5 in the wavenumber range 20 to 60, and around -2 in the wavenumber range 60 to 100 instead of the -1.5 and -3.5 values found for the spectra derived from the vorticity statistics (panel b). The auto-correlation of the divergent wind errors is then much whiter than the auto-correlation of the rotational wind errors.

Assuming geostrophy, the linearized geopotential P can be expressed as $P = \psi/f$ where f is the Coriolis parameter, and we get

$$B_{l,l} + B_{t,t} = -\frac{\Delta B_{P,P}}{f^2} \tag{6}$$

One can then approximate the geostrophic "kinetic energy spectra" from the P spectra by applying the Laplacian operator to the statistics. These are shown in Figure 3,d. One can clearly see the shift towards small scales introduced by the Laplacian operator (comparing with panel a). Accordingly, the slopes have also been modified. For the tropospheric levels, they are now around -1.2 in the wavenumber range 20 to 60, and around -2.5 in the range 60 to 100 (see also Table 1). The spectra peak around wavenumber 20, which agrees quite well with the spectra produced in Figure 11 of Bartello and Mitchell (1992), which peak around equivalent total wavenumber 30.

There is some similarity between the spectra derived from the vorticity statistics (Fig 3,b) and the spectra derived from the mass statistics assuming geostrophy (Fig 3,d), although the spectra have much more power than the geostrophic Kinetic energy spectra at low wavenumbers. The degree of geostrophy can be indicated by the comparison between the spectra derived from the vorticity statistics and the spectra derived from the mass statistics assuming geostrophy. The

slopes of these spectra are in good agreement in the range 20 to 60 as seen from Table I, but much less so for the finer scales. The geostrophic coupling is then seen to depend on the horizontal scale. Projecting the statistics onto the eigenvectors of the covariance matrix for vorticity also indicated a lower degree of balance for the finer vertical scales. This is a feature which had already been implemented in the Optimum Interpolation (*Lönnberg* 1988).

From the auto-correlation spectra, one can produce the auto-correlation functions in grid-point space. These are presented for the mass variable P in Fig 4. One can see how the correlation decreases as a function of distance for all selected levels. These correlations drop to almost 0 at a distance of about 2000 to 3000 km, which corresponds fairly well to the results presented in Fig 3 in *Balgovind et al* (1983). In particular, there is a good agreement between our auto-correlation function at level 18 (500 hPa) and their statistics in the latitude band 40 to 50 degrees. The correlation scale is larger for the "stratospheric" levels. In Fig 5, the same auto-correlation functions are plotted for very large distances (solid lines). One can notice some positive values occurring at a very large distance, which would indicate that an error is positively correlated with the antipode. This feature of the statistics is not understood and does not appear to be realistic. As explained in part I, one possible way to eliminate the noise at the antipode would be to reset the correlation to zero beyond a certain distance, thus obtaining compactly supported correlations. An illustration of the impact of this re-setting to zero after a distance of approximately 4000 km is presented in Fig 5 (dashed curves). Hardly any change is noticeable for short distances. The impact on the spectra is shown in Fig 6. The compactly supported correlations (dashed lines) are very similar to the original ones (solid lines), apart from the fact that the modified spectra are much smoother and not as noisy. Although this has not been implemented in the operational statistics for the time being, it is likely to be beneficial.

The spectra presented above were shown up to wavenumber 106. However, in practice, the current resolution of the 3D-Var system is using these statistics only up to wavenumber 63. For this reason, all the results presented in the following will be truncated to 63, in order to provide a faithful illustration of the operational system.

As in Part I, one can define a length-scale characteristic of the curvature at the origin for an auto-correlation function. These length-scales were computed for the mass variable P, for temperature T and specific humidity Q at each level. They are presented in Fig 7 and Table 2 (the modified P variable will be discussed in section 4). The length-scales for Q and T are fairly constant in the troposphere at around 250 and 280 kilometres respectively, with an increase in the stratosphere (It should be noted that the forecasts used to produce these statistics were based on Optimum Interpolation analyses for which the stratospheric humidities were set to a constant value. Results relative to stratospheric humidities are therefore not believed to be very relevant). The mass variable P exhibits different behaviour, with a large increase from a value of 500 km at 400 hPa to a value approaching 900 km at the top of the model. This profile for P fits the equivalent figure (Fig 6) in LH86 reasonably well (with a factor 2 difference, corresponding to different definitions of the length-scales). An interesting aspect of these curves is the fact that the temperature has a shorter length-scale than the mass variable P. This had already been noted by *Phillips* (1986) for his statistics of a random ensemble of slow modes, and is a consequence of the geostrophy, and the resulting invalidity of the separability assumption. The auto-correlation spectra presented in Fig 3 already indicate that the horizontal correlations vary with level. Another illustration of non-separability will be given in the following section on the vertical correlations.

3c Vertical correlations

The global vertical correlations for different variables are presented in Fig 8 for four selected levels: level 6 (roughly 100 hPa), level 10 (roughly 200 hPa), level 18 (roughly 500 hPa) and level 26 (roughly 850 hPa). A measure of the sharpness of the correlations is also computed as the mean distance for which the correlation falls to 0.5 (in Lnp units). This measure was computed for the four levels and all variables. Results are shown in Table 3. Figure 8,a shows the vertical correlations for temperature. One notices the presence of a negative lobe for each of these correlations. For instance, level 200 hPa is positively correlated with levels above 300 hPa, but negatively correlated with levels below 300 hPa. The opposite is true for levels 500 and 850 hPa, which are positively correlated with levels below 300 hPa and negatively with levels above. It then seems that level 300 hPa is a mean "tropopause" level for our statistics, a level where a change of

sign occurs. This is consistent with the vertical correlations for thicknesses in LH86 (their Fig 13). The cross-correlation between surface pressure and temperature at all levels is presented in Fig 8,b. It shows that the surface pressure is negatively correlated with temperature in the lower troposphere and at the tropopause level (this will be discussed in Part III). In Fig 8,c, the vertical correlations for mass variable P appear to be broader than the ones for temperature in panel a (this is also easily seen from Table 3). This can be understood by the fact that P is the vertical integral of T. The vertical correlation for level 200 hPa can be compared to Fig 9 in LH86. They agree reasonably well, although our statistics are generally broader. This can be explained by the fact that in our set of statistics, there is more contribution from the Southern Hemisphere (where standard-deviations are large) than from the Northern Hemisphere. The broader correlations from the data-poor areas in the Southern hemisphere might then dominate the results.

The correlations for the rotational part of the wind and the divergent part of the wind are presented in Fig 8, panels d and e respectively. Figure 8, panel d can be compared with Fig 15 in HL86, which again exhibits slightly sharper correlations than ours. It can be noted that the vertical correlations for the rotational component of the wind (Fig 8, panel d) are sharper than those for the mass variable P (Fig 8, panel c). This result was also found in Phillips (1986), and is again a consequence of geostrophy and the invalidity of the separability assumption. Comparing the correlations for rotational and divergent parts of the wind, the statistics for the divergent part appear clearly sharper, with in particular some negative lobes (as in Fig 19 of HL86), interpreted as the manifestation of baroclinic processes within the troposphere. The last panel in Fig 8, panel f shows the correlations for the specific humidity variable. These remain positive at all levels. A small kink is visible in the 500 hPa profile at level 28 (roughly 950 hPa), corresponding to the top of the boundary layer. This might be associated with the representation of physical processes in the model. There is also an indication of a very strong vertical gradient of specific humidity around this level in the TOGA COARE dataset examined by *Johnson et al* (1996), which might affect the statistics.

The variation of the vertical correlations as a function of horizontal wavenumber is now investigated. Figure 9 presents the vertical correlations at level 18 (500 hPa) for different variables and selected wavenumbers (10,25,40,55). In all panels, the sharpening of the vertical correlations with higher wavenumbers is obvious. This represents a sort of three-dimensional isotropy: short horizontal scales are associated with short vertical scales.

This variation allows us to understand the overall sharper vertical correlation for rotational wind than for mass. As the horizontal spectra for wind are more weighted towards the smallest scales than for mass, the global (wavenumber averaged) vertical correlation will be more influenced by small structures. This illustration of the lack of separability was also found to a lesser extent in HL86 (Fig 15) and LH86 (Fig 9). The signal appears so strongly in our results that it was decided to implement such a variation of vertical correlations with respect to wavenumber in the 3D-Var structure functions, thus obviating the separability assumption.

4. PRACTICAL IMPLEMENTATION

In the previous section, the statistics obtained with the NMC method have been presented for all variables. In particular mass and wind statistics were presented separately, and it was shown that they agreed quite well with the literature, and in particular with Phillips' results on an ensemble of slow modes. In practice, it was chosen to use only the mass statistics and derive the wind statistics from them in order to have an internally consistent set of statistics, with full control over the degree of geostrophy one wants to introduce in the covariances. (Note: it was found that, when using wind statistics directly, the balanced part of the mass linked to the vorticity statistics exhibited some noise in the kernel of the operator transforming (T, P_s) into P. This noise was easier to control when using mass statistics and deriving wind statistics from them). The important things we want to insist on in the resulting statistics are geostrophy and non-separability following Phillips' ideas.

As a result, both mass and wind vertical and horizontal correlations specified in the 3D-Var system are derived from the covariances for temperature and surface pressure obtained with the "NMC method". Both the auto-correlation spectra at

all horizontal levels and the vertical correlations for each horizontal wavenumber are used with only a small modification (values for wavenumbers 0 and 1 are replaced by the values for wavenumber 2, as these statistics were too noisy). The linearised integration of the hydrostatics, to calculate P from T and $\ln p_s$ allows the computation of some mass covariances for each wavenumber n. It turns out that these covariances, especially for small n, do not drop off towards zero over large vertical separations. In terms of correlations, there is, for many large wavenumbers, an increase in the correlation $V_n^{3l,1}$ with decreasing l (higher level) in the stratosphere. This is partly due to the assumption of three-dimensional isotropy (temperature error structures tend to slope in the vertical, which we cannot take into account here). In any case, it is believed to be un-physical and in practice the correlations will be forced to go to zero, with a small adjustment of the temperature and surface pressure standard deviations. Physically, the condition is that the effect on height at the top level from a change in surface pressure has to be perfectly compensated by an opposite change in the vertical integral of temperature. The adjustment necessary for this condition to hold is, for almost all wavenumbers, a 10% reduction in the surface pressure standard deviation and a 10% increase in the temperature standard errors. For the largest horizontal scales, a larger adjustment (up to 30%) is needed. It is conceivable that for the largest scales the height correlations between the surface and the top of the model should be non-zero. However, for the time being, we enforce the condition for all wavenumbers before applying the linearized hydrostatic operator. The resulting vertical correlations for various wavenumbers at level 18 are shown in Fig 10. These are sharper than the previous ones shown in Fig 7 panel c. Another comparison with computed statistics can be found in Fig 1,a and Fig 7 where the modified P variable (long dashed lines) should be compared to the original P variable (dashed lines). The tropospheric values are seen to be in relatively good agreement, but larger differences occur in the stratosphere. The resulting statistics are believed to be a good approximation of geopotential error statistics, as can be judged from the comparison of the resulting standard-deviations and of directly computed values extracted from the earlier study of Rabier and McNally (1993). As an example, the standard-deviations for our modified mass variable and directly computed geopotential statistics are respectively 12 and 14 metres at 850 hPa, with identical values of 19 m at 500 hPa and of 22 m at 200 hPa. The modified mass statistics will be used for both the balanced part of the mass and the unbalanced part of the mass (as explained in Part I).

The next step is to derive some wind statistics from the mass statistics, using geostrophy. As for mass, these statistics will then be used for both the balanced and unbalanced parts of the wind. This is obviously a very crude approximation, as we have seen in the previous sections how different the statistics for the rotational and the divergent parts of the wind were, but it was found to be necessary for a satisfactory convergence of the minimization.

The degree of balance as a function of scale (which was observed from the statistics) is implemented in an approximate way. The variation with horizontal wavenumber is described by a linear function, which gradually decreases from 90% of the variance in the Rossby modes at wavenumber 10 to 62% of the variance in the Rossby modes at wavenumber 63. The variation with vertical mode is implemented following the simple switch from multivariate for the first 10 vertical modes to univariate for the remaining ones.

As far as the standard-deviations are concerned, the global standard-deviations at each level for temperature and the one for surface pressure are multiplied by a constant rescaling factor of 0.9, and then used in the 3D-Var system. Those for wind are derived by a simplified geostrophic relationship as explained in section 3a. In ECMWF operations, between January and September 1996, the geographical variation of standard-deviations was taken from the output of the Optimum Interpolation scheme (the index is derived from the geographical variation of geopotential errors at level 18 (500 hPa) with an inflation in the tropics). Currently, it is coming from an estimation of the analysis covariance matrix using a conjugate-gradient minimization algorithm (*Fisher and Courtier,* 1995).

For the specific humidity, our specification of the standard-deviations is not derived from the "NMC statistics" (for mainly historical reasons) but from a study of statistics of radiosonde observations minus background fields, stratified according to observed temperature and relative humidity. A simple empirical formulation for the standard-deviations of

both the background error and the observation errors was designed to model the main features of the histogram. The background errors for relative humidity are modelled as:

$$\sigma_b = -0.002T_b - 0.0033|T_b - 273| + 0.25RH_b - 0.35|RH_b - 0.4| + 0.70 \quad (7)$$

$$\sigma_b = \min(0.18, \max(0.06, \sigma_b))$$

These standard-deviations are then converted to specific humidity (ignoring the temperature contribution). As these modelled errors reproduced the data quite well for most of the troposphere but failed to reproduce the observed decrease in the values of the standard-deviations in the lower layers, they were modified in the following way: for pressure higher than P0=800 hPa and over sea, the modified standard-deviation is given by

$$\sigma_{\text{mod}} = \sigma_b(1 - a + a\exp(-((p - p_0)/b))) \quad (8)$$

where a=0.5 and b=12500. The resulting standard-deviations are presented in Fig 11, both globally (solid line) and for the Tropics (dashed line).

A problem of slow increase in the stratospheric humidity emerged in the 3D-Var data assimilation suite. This was found to be due to systematic humidity observation departures in the troposphere and small but non-zero correlations between the troposphere and the stratosphere. The solution consisted in setting the standard-deviations to a very low value above 150 hPa and setting to zero the correlations between levels above 100 hPa and all other levels. The humidity in the stratosphere in the current system is then mainly driven by the model, and not controlled by observations.

5. DISCUSSION

In this paper, background error statistics have been investigated using the differences between two forecasts valid at the same time, following a method introduced by *Parrish and Derber* (1992). This method is relatively easy to implement and provides some information for all variables and scales used in a variational system. Results compare satisfactorily with the existing literature. The simplicity of the method and its reasonable results make it a suitable tool for centres developing statistics for a variational scheme. Apart from the NCEP and ECMWF centres, it has also been used at Bureau of Meteorology Research Centre by *Steinle et al* (1995), Météo-France by *Desroziers et al* (1995), Recherche en Prévision Numérique by Gauthier (pers. comm.) and United Kingdom Meteorological Office by *Ingleby et al* (1996).

The results obtained in this study highlighted the non-separability of the statistics, with different horizontal correlations at different levels, and different vertical correlations for different horizontal wavenumbers. In particular, a kind of three-dimensional isotropy has been observed, with the sharpening of vertical correlations when going to smaller horizontal scales. Taking into account this non-separability leads to some attractive features which were not present in the separable formulation of the statistics used in the Optimum Interpolation system, such as the increase of length-scale with height for the mass variable, a shorter length-scale for temperature than for mass, sharper vertical correlations for wind than for mass. The practical importance of these features is illustrated in Part III. These three features have already been described and explained in *Phillips* (1986), but have not previously been fully implemented in an operational Optimum Interpolation analysis scheme. One should note, however, that a non-separable model of forecast error covariances can also be obtained from data statistics as shown in *Bartello and Mitchell* (1992).

The use of the same correlations at all geographical locations is a clear limitation of our implementation of the statistics. It is known that horizontal correlations get sharper with higher latitudes (*Lindzen and Fox-Rabinovitz,* 1989; *Balgovind et al* 1983). These can also vary considerably with observation network density as shown in *Daley* (1992). There is also some evidence of a clear tightening of the vertical correlations in the tropics, as can be seen in Fig 12 representing the

zonally averaged temperature correlations obtained with the "NMC method". None of these features is represented in the current formulation. However, some work is under way to introduce a latitudinal variation of vertical correlations and to describe more accurately the geographical variation of standard-deviations in a simplified Kalman filter context (Fisher and Courtier 1995)

Despite these limitations, the current implementation of the statistics obtained with the "NMC method" has been shown to be generally reasonable and the specification of non-separable statistics has had a clear positive impact on the assimilation of all data, as will be described in the next part of this paper. As shown by *Andersson et al* (1993), these non-separable structure functions are desirable for the combined use of broad temperature information from TOVS radiances and sharp wind information from conventional data. Further improvements of the method will introduce better geographical description of the background error statistics in the near future.

Acknowledgements:

We are grateful to staff at ECMWF in the data assimilation and satellite sections for their comments on the structure functions used. This work benefitted from discussions with people using the "NMC method" elsewhere and in particular John Derber, Peter Steinle, Bruce Ingleby, Gérald Desroziers and Pierre Gauthier. Carole Edis-Williams efficiently typed the manuscript.

References:

Andersson, E, J Pailleux, J R Eyre, A P McNally, G A Kelly, P Courtier and F Rabier, 1993: Assimilation of satellite data by 3D-Var at ECMWF. In: Proceedings of the ECMWF Seminar, September 1993, 167-188.

Andersson, E, J Haseler, P Undén, P Courtier, G Kelly, D Vasiljevic, C Brankovic, C Cardinali, C Gaffard, A Hollingsworth, C Jakob, P Janssen, E Klinker, A Lanzinger, M Miller, F Rabier, A Simmons, B Strauss, J-N Thépaut, and P Viterbo, 1998: The ECMWF implementation of three dimensional variational assimilation (3D-Var). Part III: Experimental results. ECMWF Techn.Memo.No.243. Submitted to Q J R Meteorol Soc.

Balgovind, R, A Dalcher, M Ghil and E Kalnay, 1983: A stochastic-dynamic model for the spatial structure of forecast error statistics. Mon Wea Rev, **111**, 701-722.

Bartello, P and H L Mitchell, 1992: A continuous three-dimensional model of short-range forecast error covariance. Tellus, **44A**, 217-235.

Boer, G J, 1983: Homogeneous and isotropic turbulence on the sphere. J atmos Sci, **40**, 154-163.

Bouttier, 1994: Sur la prévision de la qualité des prévisions météorologiques. Thèse de doctorat de l'Université Paul Sabatier à Toulouse, 240 pp.

Courtier, P, E Andersson, W Heckley, J Pailleux, D Vasiljevic, M Hamrud, A Hollingsworth, F Rabier, M Fisher, 1998: The ECMWF implementation of three dimensional variational assimilation (3D-Var). Part I: Formulation. ECMWF Techn.Memo.No.241. Submitted to Q J R Meteorol Soc.

Daley, R, 1991: Atmospheric Data Analysis. Cambridge University Press, 457 pp.

Daley, R, 1992: Forecast-error statistics for homogeneous and inhomogeneous observation networks. Mon Wea Rev, **120**, 627-643.

Desroziers, G, V Mathiot and F Orain, 1995: A study of ARPEGE forecast error covariances. Proceedings of the WMO second international symposium on assimilation of observations in meteorology and oceanography, Tokyo, Japan, Vol I, 263-268.

Downton, R A and R S Bell, 1988: The impact of analysis differences on a medium-range forecast. Meteorological Magazine, **117**, 279-285.

Eyre, J R, G Kelly, A P McNally, E Andersson and A Persson, 1993: Assimilation of TOVS radiance information through one-dimensional variational analysis. Q J R Meteorol Soc, **119**, 1427-1463.

Fisher, M and P Courtier, 1995: Estimating the covariance matrices of analysis and forecast error in variational data assimilation. ECMWF Research Department Technical Memorandum No 220, August 1995, 26 pp.

Ghil, M, S Cohn, J Tavantzis, K Bube and E Isaacson, 1981: Applications of estimation theory to numerical weather prediction. In: Dynamic meteorology: data assimilation methods, L Bengtsson, M Ghil and E Kallen, eds. (New-York: Springer-Verlag), pp. 139-224.

Hollingsworth, A, A C Lorenc, M S Tracton, K Arpe, G Cats, S Uppala, and P Kållberg, 1985: The response of NWP systems to FGGE level IIb data. Part I: Analyses. Q J R Meteorol Soc, **111**, 1-66.

Hollingsworth, A and P Lönnberg, 1986: The statistical structure of short-range forecast errors as determined from radiosonde data. Part I: The wind field. Tellus, **38A**, 111-136.

Hollingsworth, A, 1989: The verification of objective analysis: diagnostics of analysis system performance. Meteorology and Atmospheric physics, **40**, 3-27.

Ide, K, A Bennet, P Courtier, M Ghil and A Lorenc, 1996: Unified notations for data assimilation: operational, sequential and variational. J Met Soc, Japan, submitted.

Ingleby, N B, A C Lorenc, D M Barker, P L F Andrews and S Thurlow, 1996: Forecast error covariances for a variational analysis sytem. Proceedings of the AMS conference. August 1996.

Johnson, R H, P E Ciesielski, and K A Hart, 1996: Tropical inversions near the 0C level, J Atmos Sc, **51**, 1838-1854.

Lindzen, R S and M Fox-Rabinovitz, 1989: Consistent vertical and horizontal resolution. Mon Wea Rev, **117**, 2575-2583.

Lönnberg, P and A Hollingsworth, 1986: The statistical structure of short-range forecast errors as determined from radiosonde data. Part II: The covariance of height and wind errors. Tellus, **38A**, 137-161.

Lönnberg, P, 1988: Developments in the ECMWF analysis system. Proceedings of the ECMWF seminar "Data assimilation and the use of satellite data", Vol I, 75-120.

Parrish, D F and J C Derber, 1992: The National Meteorological Center's Spectral Statistical Interpolation Analysis System. Mon Wea Rev, **120**, 1747-1763.

Phillips, N A, 1986: The spatial statistics of random geostrophic modes and first-guess errors. Tellus, **38A**, 314-322.

Rabier, F and A Mc Nally, 1993: Evaluation of forecast error covariance matrix. ECMWF Research Department Technical Memorandum No195, September 1993, 30 pp.

Rabier, F, Klinker, E, Courtier, P and A Hollingsworth, 1996: Sensitivity of forecast errors to initial conditions. Q J R Meteorol Soc, **122**, 121-150.

Simmons, A J, 1991: Development of a high-resolution, semi-Lagrangian version of the ECMWF forecast model. Proceedings of the ECMWF seminar "Numerical methods in atmospheric models", Vol II, 281-324.

Steinle, P, R Seaman, W Bourke and T Hart, 1995: A generalized statistical intrepolation scheme. Proceedings of the WMO second international symposium on assimilation of observations in meteorology and oceanography, Tokyo, Japan, Vol I, 205-208.

Steinle, P, R Seaman, W Bourke and T Hart, 1995: A generalized statistical intrepolation scheme. Proceedings of the WMO second international symposium on assimilation of observations in meteorology and oceanography, Tokyo, Japan, Vol I, 205-208.

	slope in range 20-60	slope in range 60-100
Level 6 (100 hPa) variable P	-2.8	-4.0
Level 10 (200 hPa) variable P	-3.5	-3.6
Level 18 (500 hPa) variable P	-3.2	-4.7
Level 26 (850 hPa) variable P	-3.1	-4.4
Level 6 (100 hPa) KE derived from vo	-2.2	-5.9
Level 10 (200 hPa) KE derived from vo	-2.2	-4.0
Level 18 (500 hPa) KE derived from vo	-1.5	-3.7
Level 26 (850 hPa) KE derived from vo	-1.4	-3.3
Level 6 (100 hPa) KE derived from D	-1.2	-5.0
Level 10 (200 hPa) KE derived from D	-1.0	-2.9
Level 18 (500 hPa) KE derived from D	-0.6	-2.3
Level 26 (850 hPa) KE derived from D	-0.9	-1.9
Level 6 (100 hPa) KE derived from P	-0.8	-2.0
Level 10 (200 hPa) KE derived from P	-1.5	-1.6
Level 18 (500 hPa) KE derived from P	-1.2	-2.7
Level 26 (850 hPa) KE derived from P	-1.1	-2.4

Table 1: Slopes of the auto-correlation spectra for different variables at selected levels and different wavenumber ranges

		length-scales (in kms)
Level 6 (100 hPa)	variable P(modified P)	680 (710)
Level 10 (200 hPa)	variable P (modified P)	635 (647)
Level 18 (500 hPa)	variable P (modified P)	502 (493)
Level 26 (850 hPa)	variable P (modified P)	514 (517)
Level 6 (100 hPa)	Temperature	291
Level 10 (200 hPa)	Temperature	301
Level 18 (500 hPa)	Temperature	285
Level 26 (850 hPa)	Temperature	274
Level 6 (100 hPa)	Temperature	290
Level 10 (200 hPa)	Temperature	255
Level 18 (500 hPa)	Temperature	258
Level 26 (850 hPa)	Temperature	252

Table 2: Length scales of the auto-correlation functions for different variables at selected levels

	mean distance for which the correlation falls to 0.5 (in Delta ln*p*)
Correlation	
for T at level 6 (100 hPa)	0.14
for T at level 10 (200 hPa)	.19
for T at level 18 (500 hPa)	.24
for T at level 26 (850 hPa)	.09
for P at level 6 (100 hPa)	.20
for P at level 10 (200 hPa)	.22
for P at level 18 (500 hPa)	.51
for P at level 26 (850 hPa)	.16
for rotational wind (divergent wind) at level 6 (100hPa)	.30 (0.09)
for rotational wind (divergent wind) at level10 (200hPa)	.52 (0.14)
for rotational wind (divergent wind) at level 18 (500 hPa)	.52 (0.13)
for rotational wind (divergent wind) at level 26 (850 hPa)	.43 (0.12)
humidity at level 6 (100 hPa)	.09
humidity at level 10 (200 hPa)	.15
humidity at level 18 (500 hPa)	.20
humidity at level 26 (850 hPa)	.12

Table 3: Measures of the sharpness of the vertical correleations for different variables and selected levels

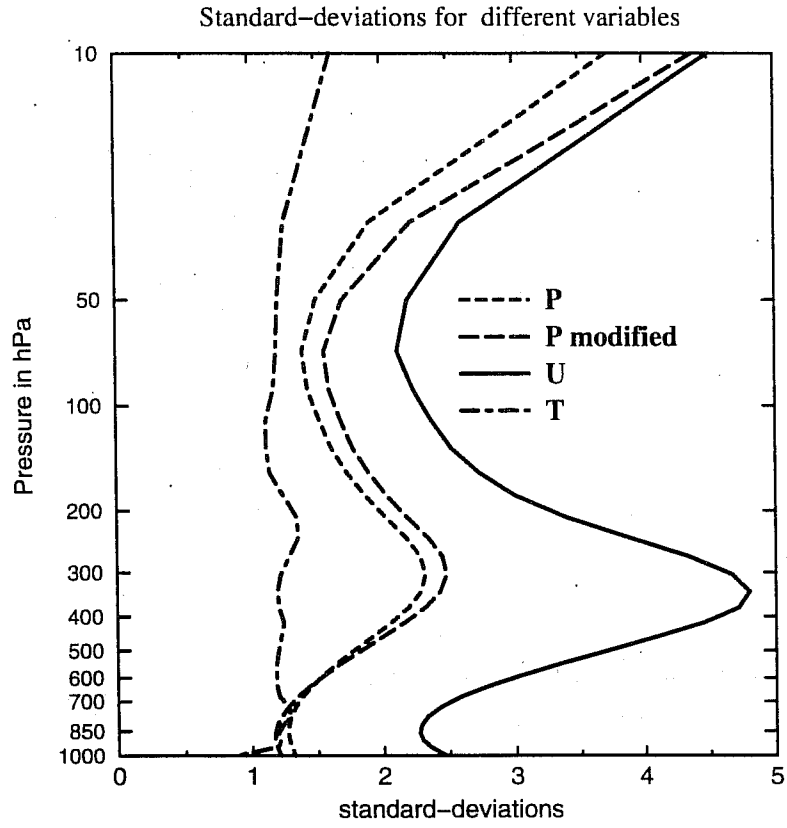

Fig 1 Horizontally averaged standard-deviations as a function of pressure (in hPa) for the mass variable P in dashed line (in 100* geopotential units), for the modified mass variable as explained in section 4 in long-dashed line (in 100* geopotential units), for the wind components in solid line (in m/s) and for the temperature in dash-dotted line (in K).

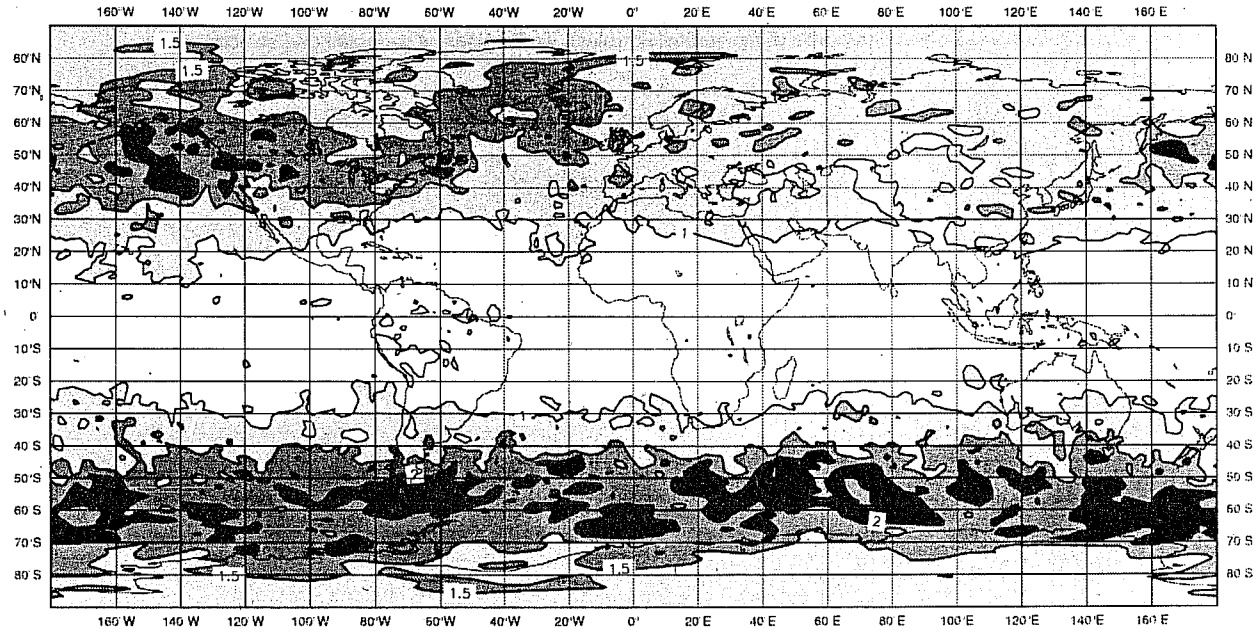

Fig 2 Geographical distribution of standard-deviations obtained with the accumulation of three months of statistics (December, January and February) for the temperature at level 500 hPa. Contours are every 0.5 K.

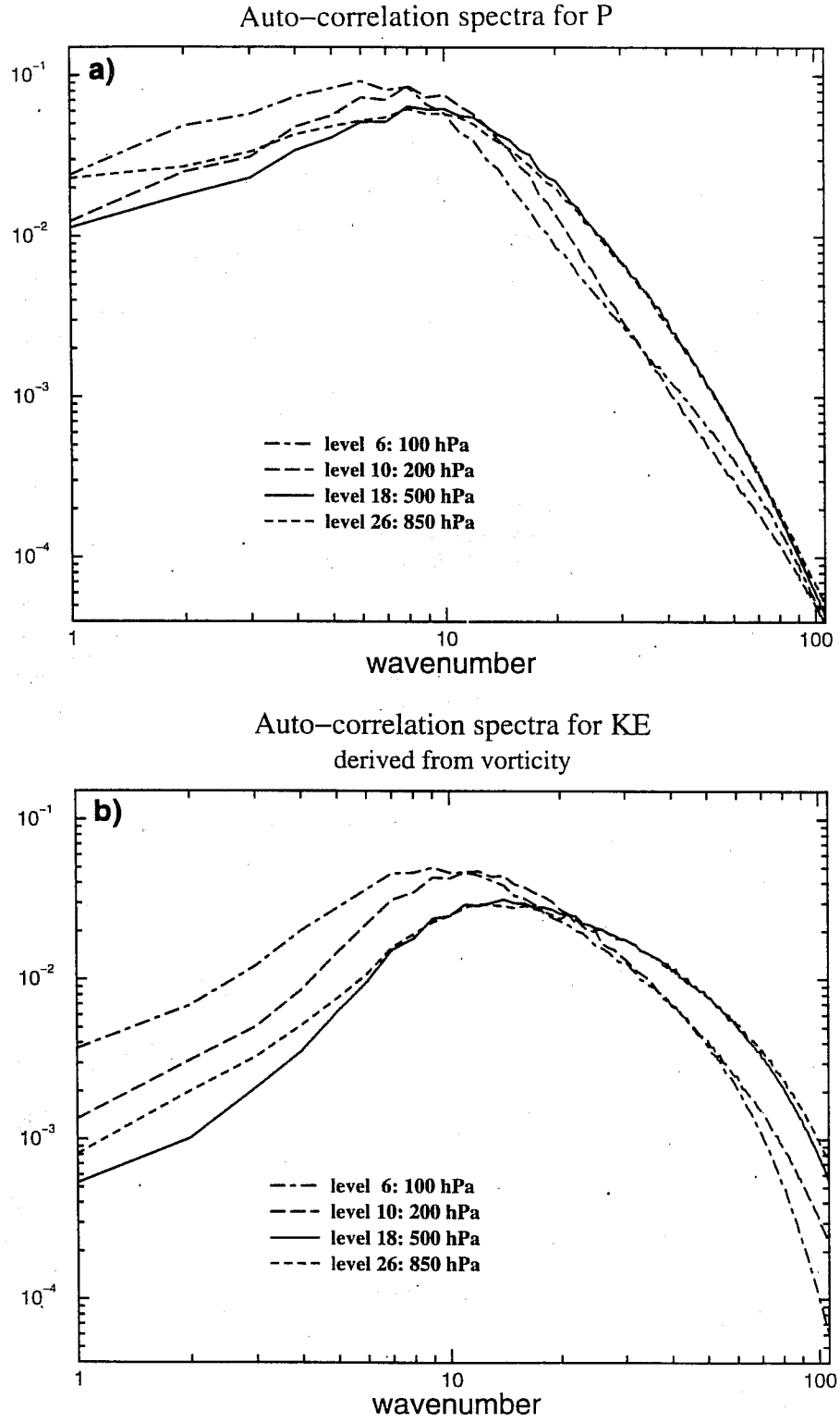

Fig 3 Horizontal auto-correlation spectra as a function of horizontal total wavenumber in a log-log graph for selected horizontal levels. Level 6 (roughly 100 hPa) is represented by a dash-dotted line, level 10 (roughly 200 hPa) by a long-dashed line, level 18 (500 hPa) by a solid line and level 26 (850 hPa) by a dashed line. Panel a is related to the mass variable P, panel b to the kinetic energy spectrum obtained from the vorticity statistics, panel c to the kinetic energy spectrum obtained from divergence statistics and panel d to the kinetic energy spectrum obtained from the P variable using geostrophy.

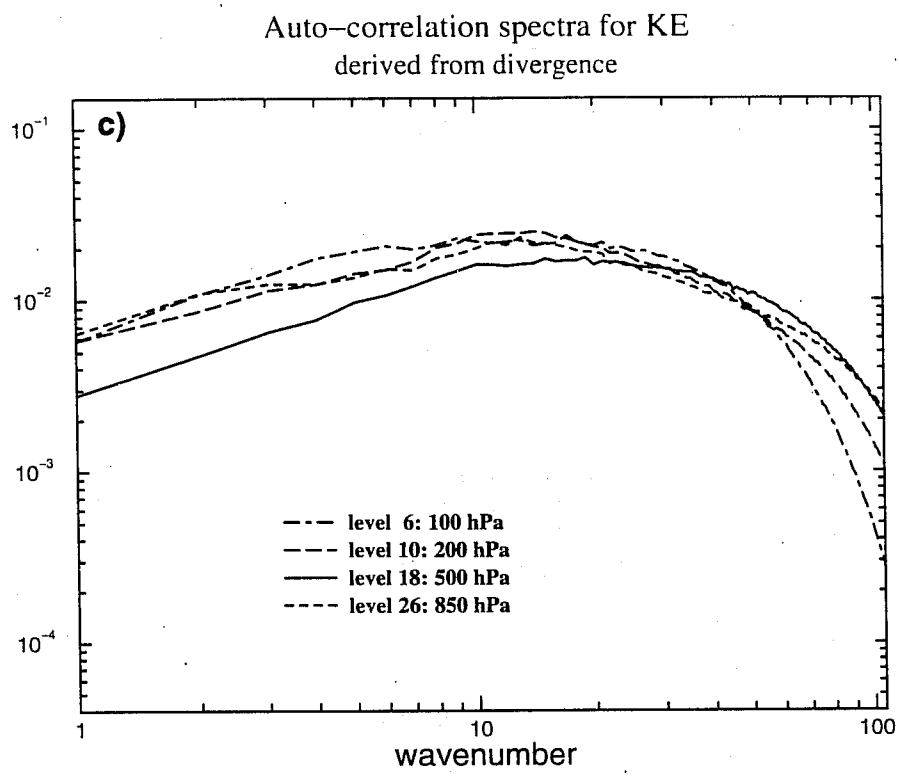

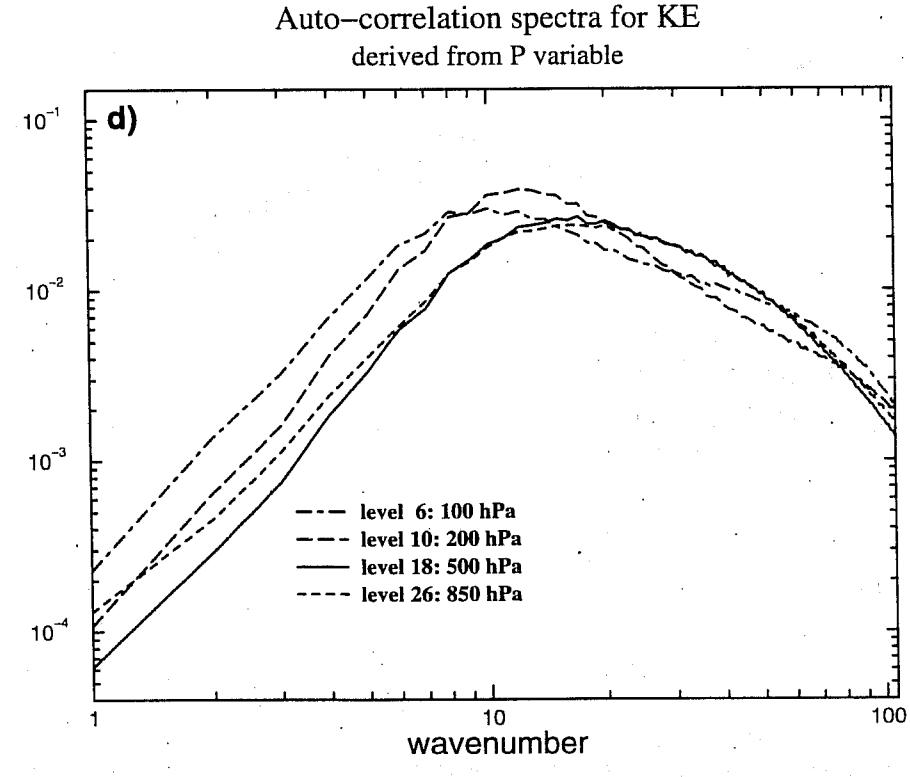

Fig 3 continued

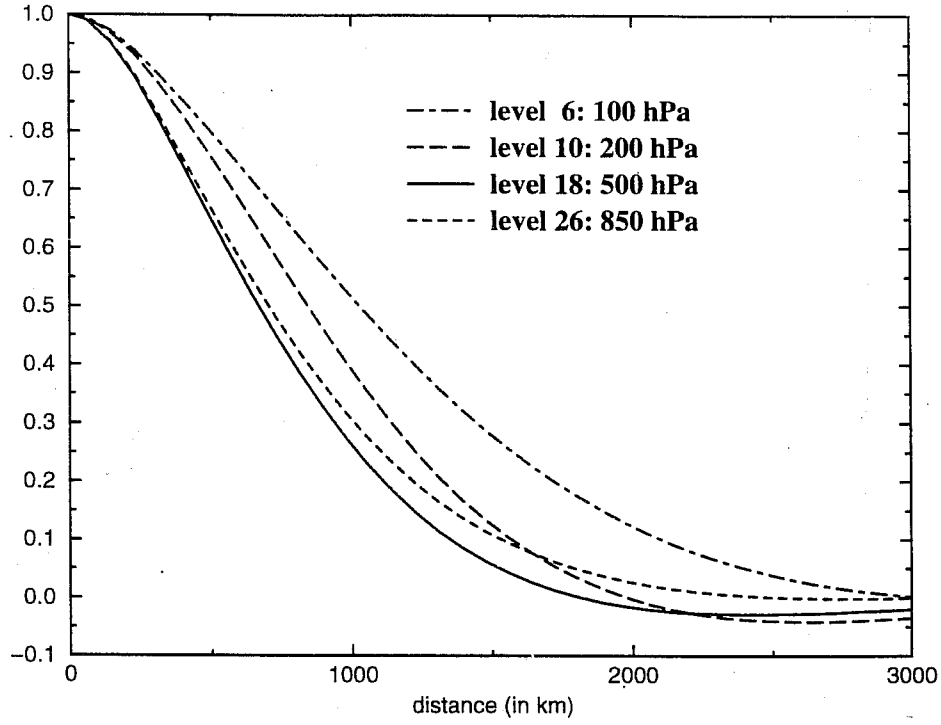

Fig 4 Horizontal auto-correlations as a function of horizontal distance for the mass variable P and selected horizontal levels. Level 6 (roughly 100 hPa) is represented by a dash-dotted line, level 10 (roughly 200 hPa) by a long-dashed line, level 18 (500 hPa) by a solid line and level 26 (850 hPa) by a dashed line.

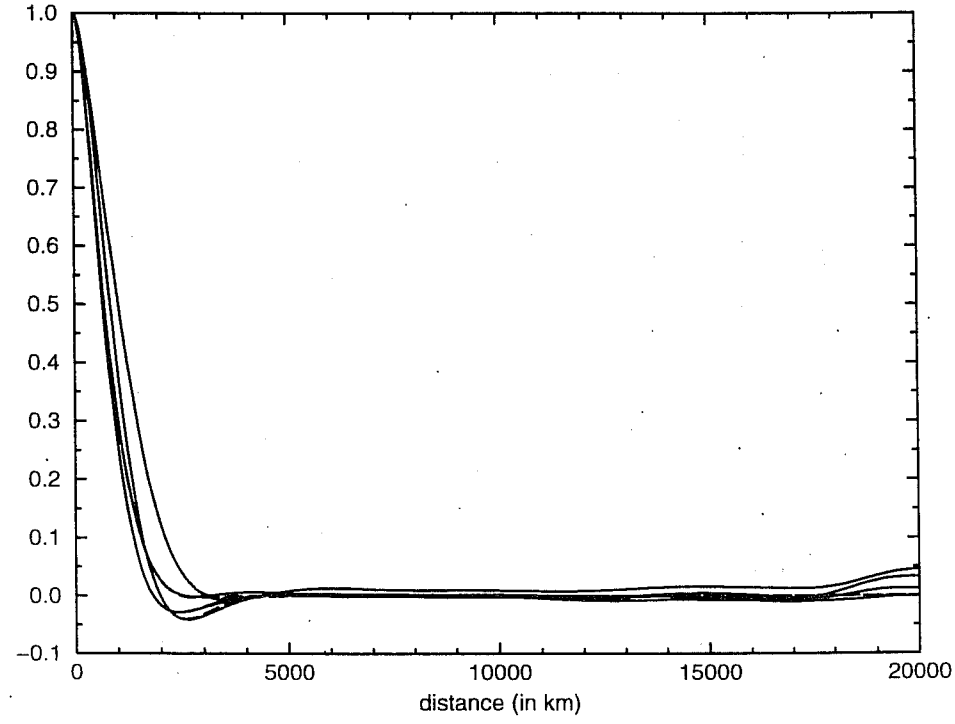

Fig 5 Horizontal auto-correlations as a function of horizontal distance up to large distances for the mass variable P and selected horizontal levels (as in Fig 2). The original curves are shown by solid lines, the compactly supported correlations obtained by resetting to zero after 4000 km are shown by dashed lines.

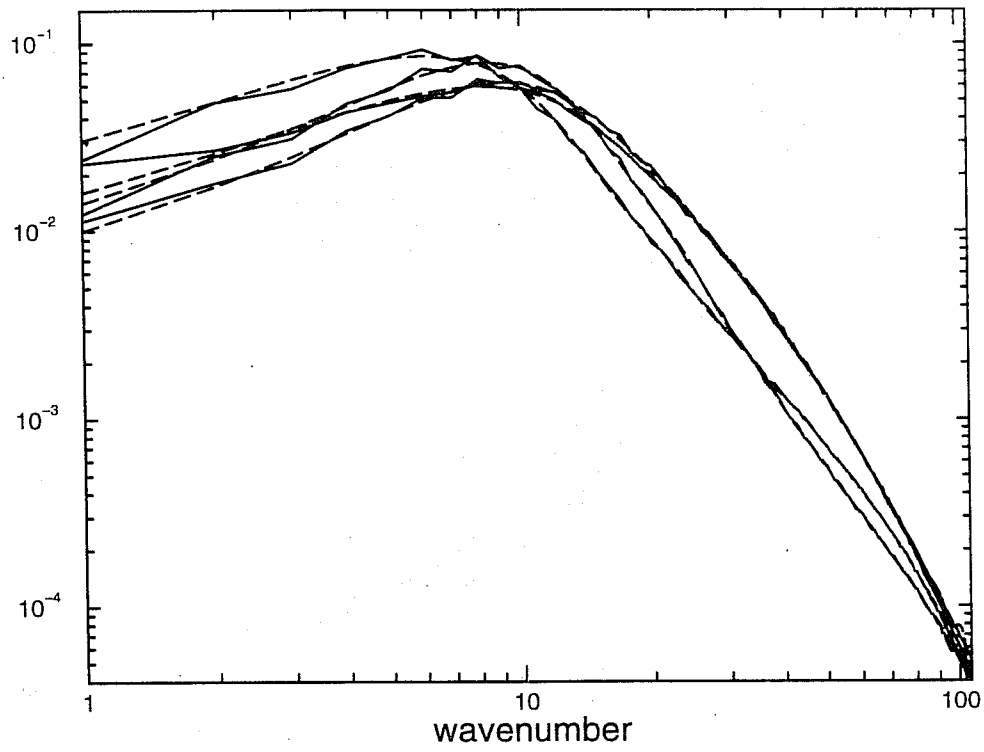

Fig 6 Horizontal auto-correlation spectra as a function of horizontal total wavenumber in a log-log graph for selected horizontal levels and mass variable P. The original curves are shown by solid lines, the compactly supported correlations obtained by resetting to zero after 4000 km are shown by dashed lines.

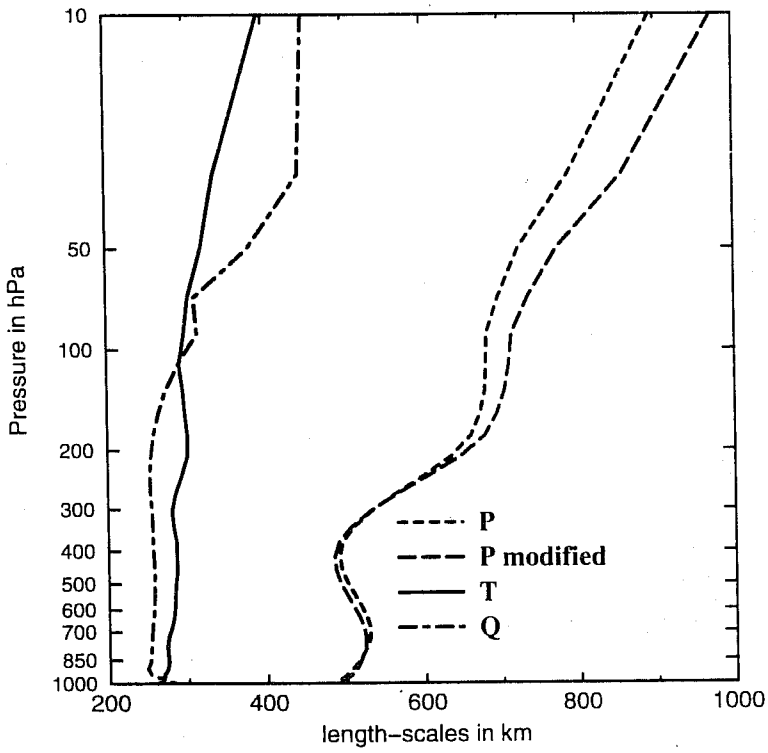

Fig 7 Horizontal length-scales (in km) as a function of pressure (in hPa) for the mass variable P (dashed line), the modified mass variable P as explained in section 4 (long-dashed line), the temperature T (solid line) and the specific humidity Q (dash-dotted line).

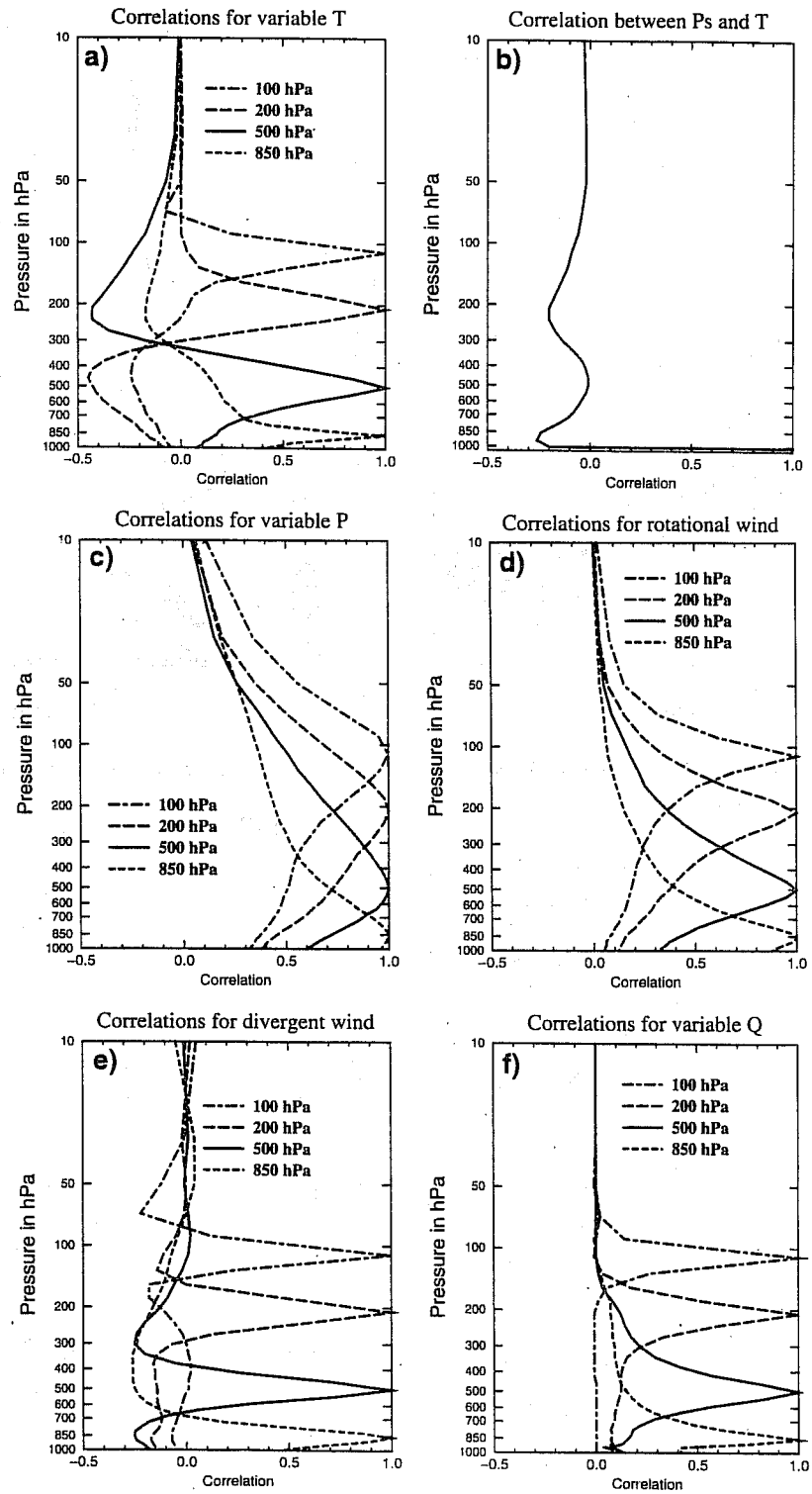

Fig 8 Global vertical correlations as a function of pressure (in hPa) for four selected levels: level 6 (roughly 100 hPa) in dash-dotted, llevel 10 (roughly 200 hPa) in long-dashed line, level 18 (roughly 500 hPa) in solid line and level 26 (roughly 850 hPa) in dashed line. Panel a shows the correlations for the temperature T, panel b the correlations between the surface pressure and the temperature (surface pressure is represented by the lowest point on the curve), panel c the correlations for the mass variable P, panel d for the rotational part of the wind, panel e for the divergent part of the wind, and panel f for the specific humidity Q.

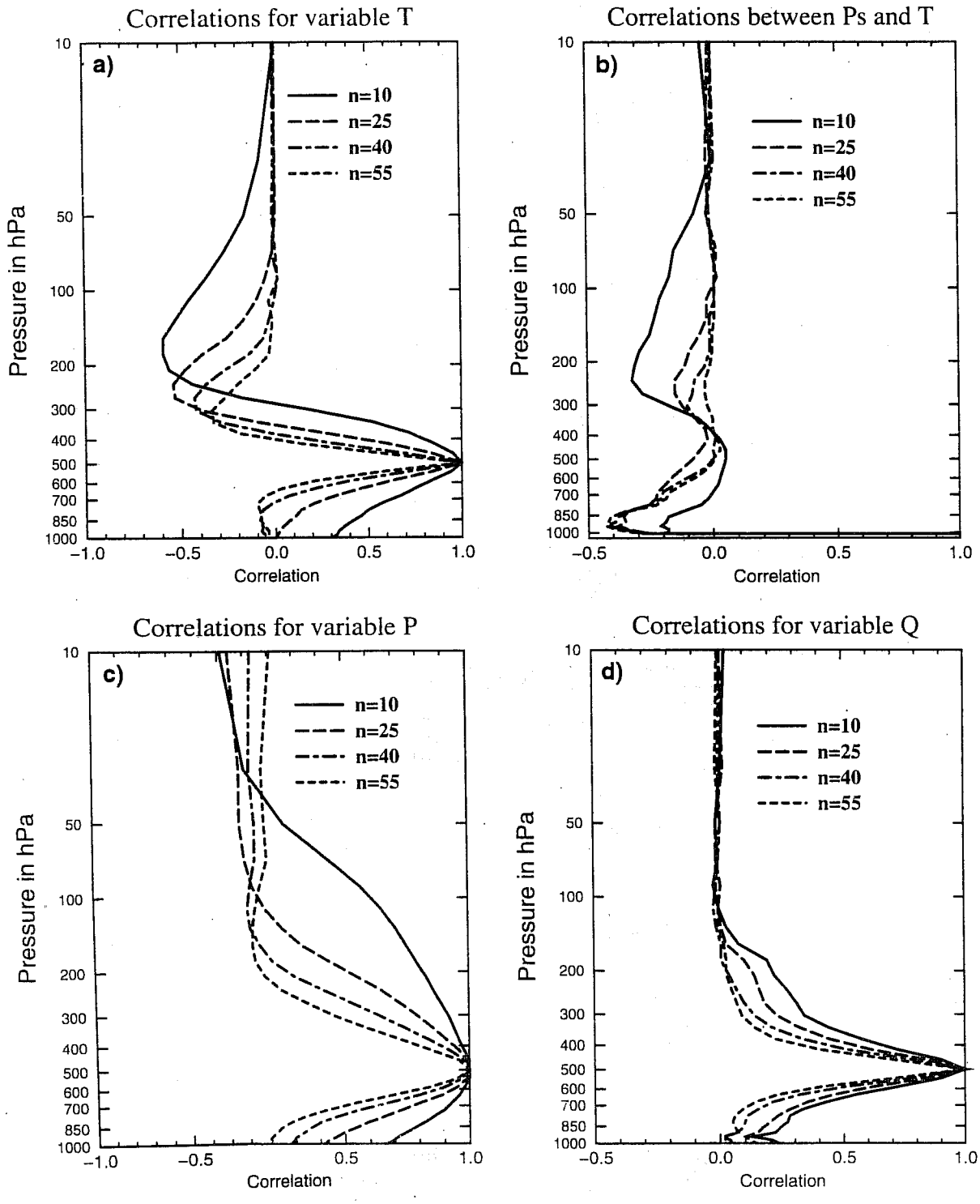

Fig 9 Vertical correlations for level 18 (roughly 500 hPa) as a function of pressure (in hPa) for selected horizontal wavenumbers. Wavenumber 10 is shown by a solid line, wavenumber 25 by a long-dashed line, wavenumber 40 by a dash-dotted line and wavenumber 55 by a dashed line. Panel a shows the correlations for the temperature T, panel b the correlations between the surface pressure and the temperature (surface pressure is represented by the lowest point on the curve), panel c the correlations for the mass variable P and panel d for the specific humidity Q.

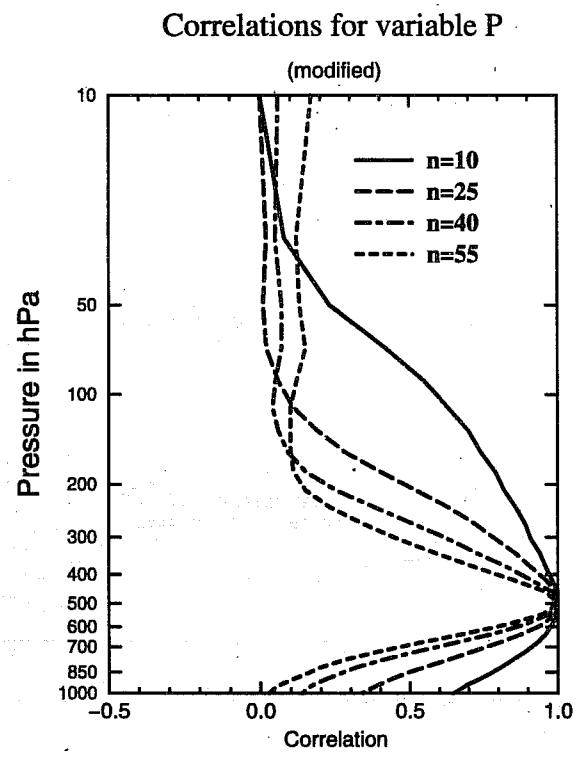

Fig 10 Vertical correlations for modified mass variable P at level 18 (roughly 500 hPa) as a function of pressure (in hPa) for selected horizontal wavenumbers. Wavenumber 10 is shown by a solid line, wavenumber 25 by a long-dashed line, wavenumber 40 by a dash-dotted line and wavenumber 55 by a dashed line.

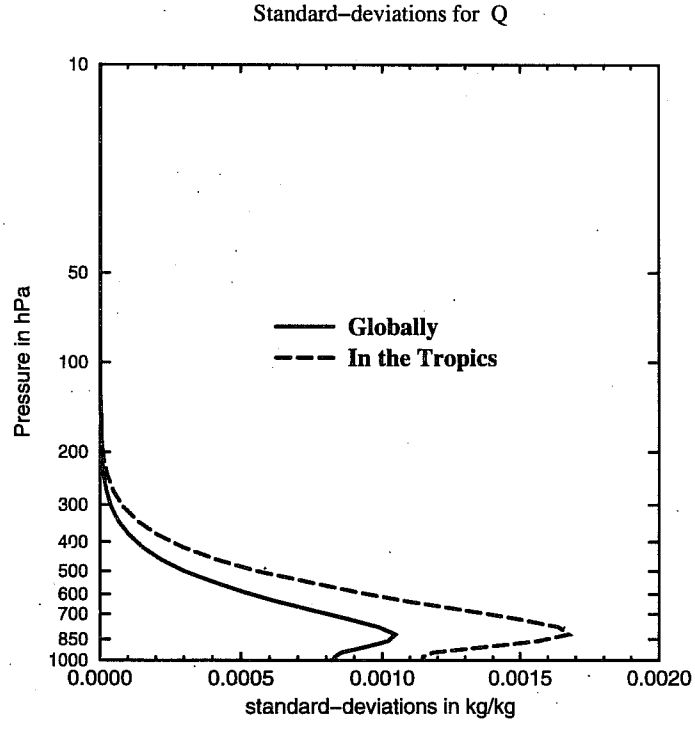

Fig 11 Horizontally averaged standard-deviations as a function of pressure (in hPa)for the specific humidity Q as a global average (solid line) and as an average over the tropical area (dashed line) in kg/kg.

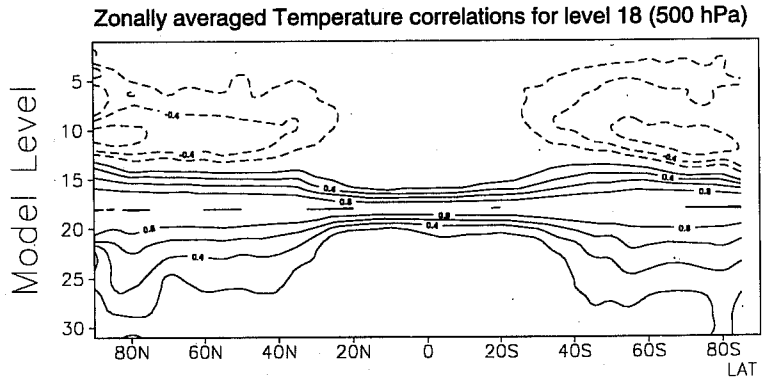

Fig 12 Zonally averaged temperature correlations for level 18 (roughly 500 hPa) as a cross-section latitude-model level. Isolines are every 0.2.